Modeling of Saturated Induction Machines With Injected High-Frequency Signals

Giovanni Bottiglieri, *Student Member, IEEE*, Alfio Consoli, *Fellow, IEEE*, and Thomas A. Lipo, *Life Fellow, IEEE*

***Abstract*—This paper analyzes the effects of injecting additional signals in induction machines for the purpose of speed control. A new saturation model able to correctly model the interaction between the added signal and saturation of the motor core due to the main torque-producing flux is presented. The introduction of a variable saturation factor is used to model the variation of the saturation level due to the additional signal. A third harmonic rotor circuit is also introduced to take account of the third harmonic component of the air-gap flux, due to saturation. An additional balanced voltage set is added to the normal supply to analyze the effects of such signals on a saturated induction motor. Simulation results of such a model both at no load and full load are presented together with experimental measurements.**

***Index Terms*—Air-gap flux harmonics, flux position estimation, q-d model, saturation modulation, sensorless control.**

I. Introduction

INJECTION of a high-frequency (hf) signal component into the current command of a voltage-source pulse width modulation (PWM) inverter is presently one of the most heavily studied and analyzed techniques for speed control of induction motors (IMs) without the need for a shaft position or speed sensor (sensorless control). It can be easily demonstrated that the injected hf signal creates additional hf voltage and current harmonics that can be used to obtain the information needed for sensorless control [1]. Among the several techniques proposed, depending on the type of the hf signal injected, it is quite interesting to analyze, in particular, the case where an additional hf symmetrical voltage component $v_{\rm shf}$ is added to the normal stator voltage. In this case, the generated hf magnetic field $F_{\rm hf}$, interacting with the main rotating field F_e, produces a periodic variation of the saturation level along the path of the magnetizing flux. In the existing techniques for sensorless control of IM, such an additional field is either rotating [1], [2] at a high angular frequency $\omega_{\rm hf}$ or pulsating on the flux axis [3] at an angular frequency $\omega_{\rm osc}$, according to the voltage set injected: rotating if $v_{s\rm hf}$ consists of a balanced set, pulsating if $v_{s\rm hf}$ is injected only in a phase or consists of three identical voltages.

Because of the increasing importance of this type of hf injection sensorless technique, it is important to analyze the effects caused by the hf injected signal on the behavior of the induction motor. Indeed, the injection of such hf voltages produces additional harmonics in the motor currents and in the stator phase-linked fluxes, causing possible noise and vibrations in the structure of the motor and a modification of its overall performance.

In order to examine the effects of additional signals on the machine, instead of studying the common cases of a pulsating or a rotating hf field, a more general case of general practical interest for sensorless control has been used. An additional field rotating at a high angular frequency $\omega_{\rm hf}$ and pulsating in amplitude at an angular frequency $\omega_{\rm osc}$ is added to the main magnetic field. As traditional d–q models of induction machines are not able to represent the phenomena produced by the injection of such an hf signal, it is necessary to introduce a new saturation model for induction machines, as will be presented and described in this paper.

II. Saturation Model

Several models describing saturation in induction motors have been presented in the recent years. One of the first approaches, proposed in [4], is to model a saturated induction machine using a small signal linearization around an operating point. A different method exploits the idea of reorienting the q–d axis to take into consideration the effect of saturation on the main flux path [5]. A more accurate model in predicting the machine performance during transient conditions introduces the effects of saturation by modifying the amplitude of the magnetizing flux λ_m with the aid of saturation factors [6], [7]. Although it is possible to take into consideration the drop of the amplitude of the saturated magnetizing flux with respect to the unsaturated one, this approach does not pay attention to the generation of higher flux harmonics in the main flux. The creation of saturation harmonics was described for the first time in [8], where their effects on the machine performance at steady state are also analyzed. An alternative approach to investigate the effects of saturation on the harmonic spectrum of the air-gap flux density is described in [9]. One of the most important facts regarding the saturation harmonics is that they all rotate at the same angular speed as the fundamental component. Therefore, it is necessary to introduce different subsystems in the motor model, one for each harmonic. However, it should be noted that the effect of the third harmonic is dominant because the amplitudes of the higher order harmonics are lower [8].

An alternative approach proposed in [10] introduces the harmonic components of the magnetizing flux due to the nonlinear nature of saturation by modifying the air-gap length as a function of the air-gap flux position and amplitude. As a consequence of saturation, a third harmonic flux component is created within the magnetizing flux, and third harmonic currents are induced in the rotor circuits creating a ripple in the total torque and

Manuscipt received August 4, 2005; revised September 29, 2006. Paper no. TEC-00267-2005.

G. Bottiglieri and A. Consoli are with the Department of Electrical, Electronic and Systems Engineering, University of Catania, 6-95125 Catania, Italy (e-mail: gbottiglieri@diees.unict.it; aconsoli@diees.unict.it).

T. A. Lipo is with the University of Wisconsin, Madison, WI 53706-1481 USA (e-mail: lipo@engr.wisc.edu).

Digital Object Identifier 10.1109/TEC.2007.895867

producing rotor losses. Hence, it is necessary to introduce into the circuit parameters of the induction motor a third harmonic magnetizing inductance relating the main component of the flux with its third harmonic component [11]. Even if such a model is able to predict more accurately the saturation effects in terms of the harmonic content of flux and current, it is of limited practical use to describe the modifications of the saturation level introduced by an additional hf injected signal. Saturation is still introduced appropriately by defining the air-gap length with reference to the particular spatial distribution of the magnetizing flux, and therefore, by modifying the conventional model with constant parameters. More complex phenomena, such as the saturation modulation produced by the hf injected signal, could be modeled only by redefining the air-gap length according to the injected signal that modifies the spatial distribution of the air-gap flux. However, this added complication has been determined as unnecessary for the application to be considered.

A proper model to investigate the hf saturation involves both modifying the amplitude of the fundamental and introducing a third harmonic component of the magnetizing flux. Therefore, as conventional models of induction machines are not able to analyze the effects of interaction between the additional hf signal and saturation of the magnetic paths, an improved saturation model must be developed, which accounts for the saturation effects in the rotor and stator magnetic cores.

The model presented in this paper is based on the standard q–d model of the machine; the voltage equations for the balanced three-phase squirrel-cage induction machines in the arbitrary reference frame are follows:

$$\begin{aligned} v_{qs} &= r_s i_{qs} + \frac{1}{\omega_b}\frac{d\psi_{qs}}{dt} + \frac{\omega}{\omega_b}\psi_{ds} \\ v_{ds} &= r_s i_{ds} + \frac{1}{\omega_b}\frac{d\psi_{ds}}{dt} - \frac{\omega}{\omega_b}\psi_{qs} \\ v'_{qr} &= 0 = r'_r i'_{qr} + \frac{1}{\omega_b}\frac{d\psi'_{qr}}{dt} + \frac{(\omega-\omega_{\rm re})}{\omega_b}\psi'_{dr} \\ v'_{dr} &= 0 = r'_r i'_{dr} + \frac{1}{\omega_b}\frac{d\psi'_{dr}}{dt} - \frac{(\omega-\omega_{\rm re})}{\omega_b}\psi'_{qr} \end{aligned} \tag{1}$$

and the equations for the flux linkages from the equivalent circuits are expressed in q–d variables by

$$\begin{aligned} \psi_{qs} &= X_{ls} i_{qs} + \psi_{mq,\rm sat}\psi_{ds} = X_{ls} i_{ds} + \psi_{md,\rm sat} \\ \psi'_{qr} &= X'_{lr} i'_{qr} + \psi_{mq,\rm sat}\psi'_{dr} = X'_{lr} i'_{dr} + \psi_{md,\rm sat}. \end{aligned} \tag{2}$$

With reference to the traditional approach to simulation, where the flux linkages are considered as state variables and the currents as dependent algebraically related variables, the currents can be solved in terms of flux linkages as follows:

$$\begin{aligned} i_{qs} &= \frac{\psi_{qs} - \psi_{mq,\rm sat}}{X_{ls}} \quad i_{ds} = \frac{\psi_{ds} - \psi_{md,\rm sat}}{X_{ls}} \\ i'_{qr} &= \frac{\psi'_{qr} - \psi_{mq,\rm sat}}{X'_{lr}} \quad i'_{dr} = \frac{\psi'_{dr} - \psi_{md,\rm sat}}{X'_{lr}}. \end{aligned} \tag{3}$$

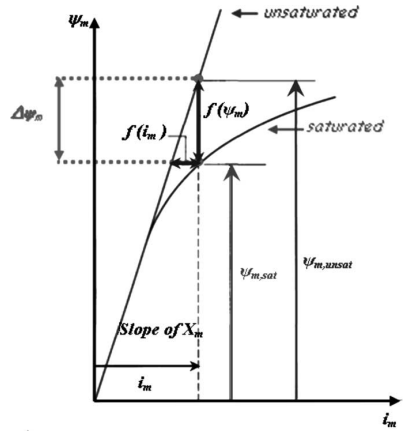

Fig. 1. Magnetization curve $\psi_m = f(i_m), \Delta\psi_m = f(\psi_{m,\rm unsat})$.

By substituting into the differential equations and integrating, one obtains

$$\begin{aligned} \frac{1}{\omega_b}\psi_{qs} &= \int\left\{ v_{qs} - \frac{r_s}{X_{ls}}\left[\psi_{qs} - \psi_{mq,\rm sat}\right] - \frac{\omega}{\omega_b}\psi_{ds}\right\} dt \\ \frac{1}{\omega_b}\psi_{ds} &= \int\left\{ v_{ds} - \frac{r_s}{X_{ls}}\left[\psi_{ds} - \psi_{md,\rm sat}\right] + \frac{\omega}{\omega_b}\psi_{qs}\right\} dt \\ \frac{1}{\omega_b}\psi'_{qr} &= \int\left\{ v'_{qr} - \frac{r'_r}{X'_{lr}}\left[\psi'_{qr} - \psi_{mq,\rm sat}\right] - \frac{\omega-\omega_{\rm re}}{\omega_b}\psi'_{dr}\right\} dt \\ \frac{1}{\omega_b}\psi'_{dr} &= \int\left\{ v'_{dr} - \frac{r'_r}{X'_{lr}}\left[\psi'_{dr} - \psi_{md,\rm sat}\right] + \frac{\omega-\omega_{\rm re}}{\omega_b}\psi'_{qr}\right\} dt. \end{aligned} \tag{4}$$

Saturation is included in the model by considering the difference between the amplitudes of the unsaturated magnetizing flux and the saturated flux, as shown in Fig. 1, which is defined with the aid of the saturation factors k_m, as described in [6] and [7]:

$$\begin{aligned} \psi_{m,\rm sat} &= \sqrt{(\psi_{mq,\rm sat})^2 + (\psi_{md,\rm sat})^2} \\ &= (1-k_m)\,\psi_{m,\rm unsat} = \psi_{m,\rm unsat} - \Delta\psi_m \end{aligned} \tag{5}$$

where $\Delta\psi_m = f(\psi_{m,\rm unsat}) = k_m\psi_{m,\rm unsat}$ and $k_m = f(\psi_{m,\rm unsat})$, the saturation factor, is a generated function of the resultant unsaturated magnetizing flux $\psi_{m,\rm unsat}$:

$$\psi_{m,\rm unsat} = \sqrt{(\psi_{mq,\rm unsat})^2 + (\psi_{md,\rm unsat})^2}$$

$\Delta\psi_{mq}$ and $\Delta\psi_{md}$ are the differences between the amplitudes of the q- and d-components of the unsaturated flux and the same components of the magnetizing saturated flux, defined by

$$\begin{aligned} \Delta\psi_{mq} &= \frac{\psi_{mq,\rm unsat}}{\psi_{m,\rm unsat}}\Delta\psi_m = k_m\psi_{mq,\rm unsat} \\ \Delta\psi_{md} &= \frac{\psi_{md,\rm unsat}}{\psi_{m,\rm unsat}}\Delta\psi_m = k_m\psi_{md,\rm unsat} \end{aligned} \tag{6}$$

and the unsaturated magnetizing fluxes on the d- and q-axis are given as

$$\psi_{mq,\mathrm{unsat}} = X_m\left(i_{qs} + i'_{qr}\right)$$
$$\psi_{md,\mathrm{unsat}} = X_m\left(i_{ds} + i'_{dr}\right). \tag{7}$$

Substituting the expressions for currents in (7)

$$\psi_{mq,\mathrm{unsat}} = \frac{X^*_{mm}}{X_{ls}}\psi_{qs} + \frac{X^*_{mm}}{X'_{lr}}\psi'_{qr} + X^*_{mm} \times \left(\frac{1}{X_{ls}} + \frac{1}{X'_{lr}}\right)\Delta\psi_{mq}$$
$$\psi_{md,\mathrm{unsat}} = \frac{X^*_{mm}}{X_{ls}}\psi_{ds} + \frac{X^*_{mm}}{X'_{lr}}\psi'_{dr} + X^*_{mm} \times \left(\frac{1}{X_{ls}} + \frac{1}{X'_{lr}}\right)\Delta\psi_{md} \tag{8}$$

where

$$X^*_{mm} = \frac{1}{\frac{1}{X_m} + \frac{1}{X_{ls}} + \frac{1}{X'_{lr}}}.$$

It is also known that, as a consequence of saturation, the resultant air-gap flux assumes a flattened sinusoidal form [10]. Its harmonic content, which includes all odd harmonics, is dominated by the third harmonic. Therefore, to analyze the harmonics of the main variables due to saturation and its effect on the added hf signal, saturation of the magnetic core cannot be modeled only by decreasing the amplitude of the main magnetizing flux. It is necessary to consider a third harmonic component rotating in the air gap with the same speed and direction, in addition to the fundamental component of the air-gap magnetizing flux. Therefore, the q–d model described before can be modified by creating third harmonic q- and d-axis components of the magnetizing flux. Such components are obtained using the well-known trigonometric triplication formula:

$$\sin(3\omega t) = 3\,\sin(\omega t) - 4[\sin(\omega t)]^3 \tag{9}$$

where $\sin(\omega\, t)$ is a sinusoidal signal pulsating at the angular frequency ω and $\sin\,(3\omega\, t)$ is a sinusoidal signal pulsating at the angular frequency $3\,\omega$.

According to (9), the additional third harmonic components are derived from the fundamental quantities by the following two analytical expressions:

$$\psi_{mq3} = \left[3\left(\frac{\psi_{mq,\mathrm{unsat}}}{\psi_{m,\mathrm{unsat}}}\right) - 4\left(\frac{\psi_{mq,\mathrm{unsat}}}{\psi_{m,\mathrm{unsat}}}\right)^3\right]\psi_{m3}$$
$$\psi_{md3} = \left[3\left(\frac{\psi_{md,\mathrm{unsat}}}{\psi_{m,\mathrm{unsat}}}\right) - 4\left(\frac{\psi_{md,\mathrm{unsat}}}{\psi_{m,\mathrm{unsat}}}\right)^3\right]\psi_{m3} \tag{10}$$

where ψ_{m3}, the amplitude of the third harmonic component of the air-gap flux, can be obtained from the amplitude ψ_m of the fundamental component of the magnetizing flux using the relation

$$\psi_{m3} = f(\psi_{m,\mathrm{unsat}}). \tag{11}$$

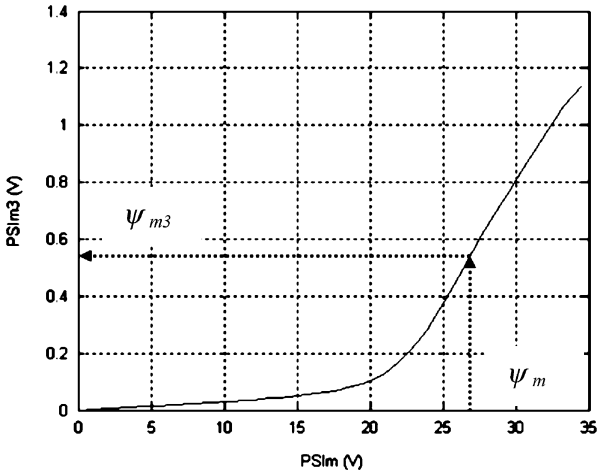

Fig. 2. Curve $\Delta\psi_{m3} = f(\psi_{m,\mathrm{unsat}})$.

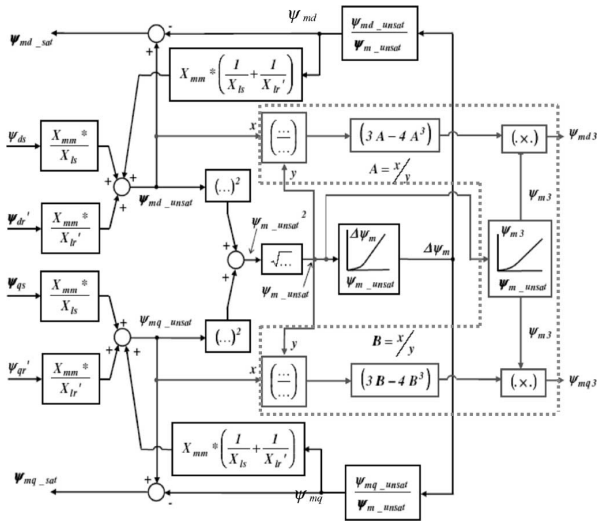

Fig. 3. Introduction of saturation in the standard q–d model.

Such a curve can be obtained from experimental tests or finite element analysis (FEA) of saturated IM models [1], [10]. In Fig. 2, the third harmonic magnetizing (air gap) flux linkage has been calculated for the machine used in this paper through FEA of the motor performance as a function of the fundamental air-gap flux linkage amplitude.

Modification of the standard q–d model due to saturation of the magnetic core, as described by (5)–(11), is shown in Fig. 3. The selected part of the scheme is used to create the additional third harmonic in the magnetizing flux, as described by (10).

The response of the rotor cage to the two components of the magnetizing flux is a cage current that has two components rotating, respectively, at the fundamental and three times the fundamental angular frequency. It is, then, necessary to model the machine with two different rotor circuits, one for the fundamental current and the other for the third harmonic current, as described in [10]:

$$i'_{qr3} = \frac{\psi'_{qr3} - \psi_{mq3}}{X'_{lr}} \qquad i'_{dr3} = \frac{\psi'_{dr3} - \psi_{md3}}{X'_{lr}} \tag{12}$$

where ψ'_{qr3} and ψ'_{dr3} are the q- and d-axis third harmonic components of the rotor flux linkages, respectively, ψ_{mq3} and ψ_{md3} are the q- and d-axis third harmonic components of the magnetizing flux linkages, respectively, i'_{qr3} and i'_{dr3} are the q- and d-axis third harmonic components of the rotor currents, respectively.

Inserting these results into the differential equations

$$v'_{qr3} = 0 = r'_r i'_{qr3} + \frac{1}{\omega_b}\frac{d\psi'_{qr3}}{dt} + 3\frac{(\omega - \omega_{\rm re})}{\omega_b}\psi'_{dr3}$$
$$v'_{dr3} = 0 = r'_r i'_{dr3} + \frac{1}{\omega_b}\frac{d\psi'_{dr3}}{dt} - 3\frac{(\omega - \omega_{\rm re})}{\omega_b}\psi'_{qr3} \quad (13)$$

and by integration, one obtains

$$\frac{1}{\omega_b}\psi'_{qr3} = \int\left\{ v'_{qr3} - \frac{r'_r}{X'_{lr}}\left[\psi'_{qr3} - \psi_{mq3}\right] - 3\frac{(\omega-\omega_{\rm re})}{\omega_b}\psi'_{dr3}\right\} dt$$
$$\frac{1}{\omega_b}\psi'_{dr3} = \int\left\{ v'_{dr3} - \frac{r'_r}{X'_{lr}}\left[\psi'_{dr3} - \psi_{md3}\right] + 3\frac{(\omega-\omega_{\rm re})}{\omega_b}\lambda'_{qr3}\right\} dt. \quad (14)$$

The torque produced by the machine also consists of two different components [10], [11]. The first is related to the interaction between the fundamental stator and rotor current components. The other one, related to the interaction between the fundamental stator and the third harmonic rotor currents, depends on the third harmonic component of magnetizing flux, which is a function of its fundamental component, as shown in Fig. 2.

$$T_{e,1} = \frac{3}{2}\frac{p}{\omega_b}X_{m,\rm sat}\left(i'_{dr}i_{qs} - i'_{qr}i_{ds}\right) \quad (15)$$

$$T_{e,3} = \frac{3}{2}\frac{p}{\omega_b}X_{sr3,\rm sat}\left[i_{qs}i'_{dr3} - i_{ds}i'_{qr3}\right] \quad (16)$$

where $2p$ is the number of poles and $X_{m,\rm sat}$, the saturated magnetizing reactance, is

$$X_{m,\rm sat} = \omega_b L_{m,\rm sat} = \omega_b(1-k_m)L_m = \frac{\psi_{m,\rm sat}}{i_m} = \frac{\psi_{mq,\rm sat}}{i_{mq}} = \frac{\psi_{md,\rm sat}}{i_{md}}$$

$X_{sr3,\rm sat}$, the mutual reactance between the stator and the third harmonic rotor circuit, is calculated from the third harmonic component of the air-gap flux.

$$X_{sr3,\rm sat} = \omega_b L_{sr3,\rm sat} = \frac{\psi_{m3}}{i_m}. \quad (17)$$

Finally, as the motor is physically connected to an external load, the equation that couples the electrical to the mechanical system is

$$T_e - T_l = \frac{2}{p}J\frac{d\omega_{\rm re}}{dt} \quad (18)$$

where $T_e = T_{e1} + T_{e3}$ is the electromagnetic torque, T_l is the load torque, and J is the inertia of the rotor.

III. Simulation Model

The model described in Section II is now used to describe the effects produced by injection of hf signals. To this aim, it is useful to consider a general case where a balanced three-phase voltage set, pulsating in amplitude at an angular frequency $\omega_{\rm osc}$ and rotating at a generic angular frequency $\omega_{\rm rot}$, is added to the normal supply

$$v_{as} = V_{\max}\cos(\omega_e t) + v_{a\rm hf}$$
$$v_{bs} = V_{\max}\cos\left(\omega_e t - \frac{2}{3}\pi\right) + v_{b\rm hf}$$
$$v_{cs} = V_{\max}\cos\left(\omega_e t + \frac{2}{3}\pi\right) + v_{c\rm hf} \quad (19)$$

where ω_e is the angular frequency of the main magnetizing field and

$$v_{a\rm hf} = \left[V_{\rm hf}\cos(\omega_{\rm osc}t)\right]\cos(\omega_{\rm rot}t)$$
$$v_{b\rm hf} = \left[V_{\rm hf}\cos(\omega_{\rm osc}t)\right]\cos\left(\omega_{\rm rot}t - \frac{2}{3}\pi\right)$$
$$v_{c\rm hf} = \left[V_{\rm hf}\cos(\omega_{\rm osc}t)\right]\cos\left(\omega_{\rm rot}t + \frac{2}{3}\pi\right) \quad (20)$$

are the added hf signals.

The magnetic field, rotating at $\omega_{\rm rot}$ and pulsating in amplitude at $\omega_{\rm osc}$, generated by such an additional signal, interacting with the main field F_e rotating at ω_e produces a modulation of the saturation level along the path followed by the magnetizing flux. Such a variation depends on the component of the additional magnetic field on the direction of the main field F_e, which is obtained by the projection of $F_{\rm hf}$ on the d-axis locked to the air-gap flux axis and rotating at ω_e :

$$(F_{\rm hf})d = \left[F_{\rm hf}\cos(\omega_{\rm osc}t)\right]\cos[(\omega_{\rm rot} - \omega_e)t]$$
$$= \frac{1}{2}F_{\rm hf}\{\cos[(\omega_{\rm rot} - \omega_{\rm osc} - \omega_e)t] + \cos[(\omega_{\rm rot} + \omega_{\rm osc} - \omega_e)t]\}. \quad (21)$$

Therefore, it is possible to assume that the magnetizing flux λ_e, rotating at an angular frequency ω_e, has its amplitude modulated by the d-component of the additional flux $\lambda_{\rm hf}$, corresponding to the field $F_{\rm hf}$.

$$\lambda_e = \left[\Lambda_e + \Lambda_{e,\rm hf}\right]\cos(\omega_e t)$$
$$\Lambda_{e,\rm hf} = \Delta\Lambda_{e,\rm hf}\cos(\omega_{\rm osc}t)\cos\left[(\omega_{\rm rot} - \omega_e)t\right]. \quad (22)$$

By trigonometric manipulation of (22), one obtains

$$\Lambda_{e,\rm hf} = \frac{1}{2}\Delta\Lambda_{e,\rm hf}\cos[(\omega_{\rm rot} - \omega_{\rm osc} - \omega_e)t] + \frac{1}{2}\Delta\Lambda_{e,\rm hf}\cos[(\omega_{\rm rot} + \omega_{\rm osc} - \omega_e)t]. \quad (23)$$

It can be noted that if $\omega_{\rm osc}$ is zero and $\omega_{\rm rot} = \omega_{\rm hf}(\gg\omega_e)$, the additional signal produces an hf field rotating at the angular

speed $\omega_{\rm hf}$ [12]. Therefore, the amplitude of the magnetizing flux that is directed along the d-axis and rotates at ω_e is made of two different components. The first component is constant and is due to the normal supply frequency, while the second one is pulsating at $\omega_0 = \omega_{\rm hf} - \omega_e$ because the projection of the hf field on the d-axis depends on the difference between the rotating speeds of the two magnetic fields.

On the contrary, if $\omega_{\rm rot} = \omega_e$, the additional signal creates an additional field rotating at the same angular frequency of the main flux and pulsating at $\omega_{\rm osc}$ in amplitude. In other words, in this case, the amplitude of the magnetizing flux includes the normal constant component due to the motor supply and an additional component pulsating at $\omega_{\rm osc}$ due to the added signal.

Finally, if $\omega_{\rm rot} = 0$, the additional signal produces a field in a constant direction pulsating in amplitude at $\omega_{\rm osc}$. In this case, the amplitude of the air-gap flux contains, in addition to the constant term, two different components pulsating, respectively, at $\omega_{\rm osc} - \omega_e$ and $\omega_{\rm osc} + \omega_e$.

Considering the voltage set in (19) and (20), and transforming it into the q–d stationary reference frame, it is possible to obtain the input voltages of the model described earlier:

$$\begin{bmatrix} v_{qs} \\ v_{ds} \\ v_{\rm os} \end{bmatrix} = \frac{2}{3} \begin{bmatrix} \cos(\gamma_s) & \cos\left(\gamma_s - \frac{2}{3}\pi\right) & \cos\left(\gamma_s + \frac{2}{3}\pi\right) \\ \sin(\gamma_s) & \sin\left(\gamma_s - \frac{2}{3}\pi\right) & \sin\left(\gamma_s + \frac{2}{3}\pi\right) \\ \frac{1}{2} & \frac{1}{2} & \frac{1}{2} \end{bmatrix} \cdot \begin{bmatrix} v_{\rm as} \\ v_{\rm bs} \\ v_{\rm cs} \end{bmatrix}$$

where $\gamma_s = \theta - \theta_s$, with θ and θ_s representing the position, respectively, of the q–d reference frame and of the a–b–c stator frame with respect to the stator phase a. As in this case, $\gamma_s = 0$, it follows

$$\begin{aligned} v_{qs} &= V_{\max}\,\cos(\omega_e t) + [V_{\rm hf}\,\cos(\omega_{\rm osc} t)]\cos(\omega_{\rm rot} t) \\ v_{ds} &= -\left\{V_{\max}\,\sin(\omega_e t) + [V_{\rm hf}\,\cos(\omega_{\rm osc} t)]\sin(\omega_{\rm rot} t)\right\}. \end{aligned} \quad (24)$$

Using the q- and d-voltages, calculated in (24), as the input voltages in (4) and solving the model described by (4)–(18), the variables of interest can be evaluated. In this way, the effects of the hf additional signal in a saturated motor structure can be analyzed and discussed both at no load and full load. In particular, it is interesting to analyze how the injection of the hf signal introduces new harmonics in the stator currents and linkage fluxes, and to check if, besides the fact that they can be used to evaluate the position of the main flux, they also modify the torque of the motor.

IV. Simulation Results

In order to validate the model, several simulations were performed, both at no load and at full load, using a 1.1 kW, three-phase induction motor. The motor data are presented in Table I.

TABLE I
Motor Parameters

Pole pairs	*2*
Rated Power	*1.1 kW*
Rated line to line Voltage	*400 V*
Rated stator frequency	*50 Hz*
Stator resistance	*7 Ω*
Stator leakage inductance	*0.02H*
Rotor resistance referred to the stator circuits	*6.6 Ω*
Rotor leakage inductance referred to the stator circuits	*0.02 H*
Magnetizing inductance	*0.5 H*

A. No Load Tests

Firstly, a simulation without injection of additional signal was performed at no load, rated flux using a 27.5 $V_{\rm rms}$, 5 Hz balanced set as supply voltages. Then, to study the effects of the additional voltages, a 20 $V_{\rm rms}$, 500 Hz balanced set of voltages modulated in amplitude at 50 Hz was added to the normal supply.

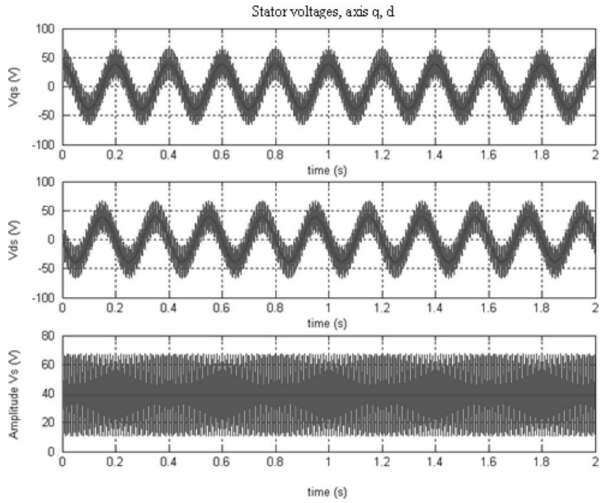

Fig. 4. Supply voltages at no load.

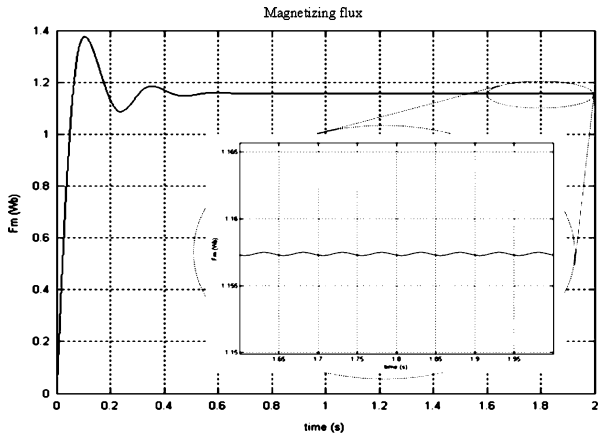

Fig. 5. Magnetizing flux λ_m without injection at no load.

Fig. 4 shows the stator voltages in the stationary reference frame (q- and d-axis rotating at $\omega = 0$) with the injection of the added signal. The amplitude of the voltage is also shown.

The injected signal (20) creates an additional magnetic field that, interacting with the main field, causes a ripple in the magnetizing flux λ_m [13]. Figs. 5 and 6 show the amplitude of the air-gap flux both without and with the additional signal.

It can be easily shown that the injection of the additional signal does not modify the mean value of the amplitude of the magnetizing flux ($\lambda_m = 1.157$) Wb, but introduces two additional harmonics, respectively, at the following angular

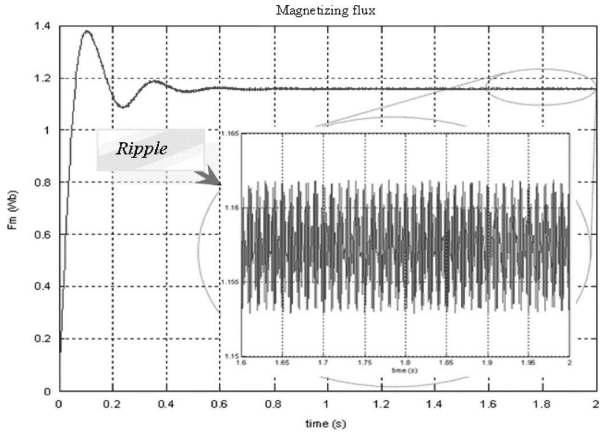

Fig. 6. Magnetizing flux λ_m with injection at no load.

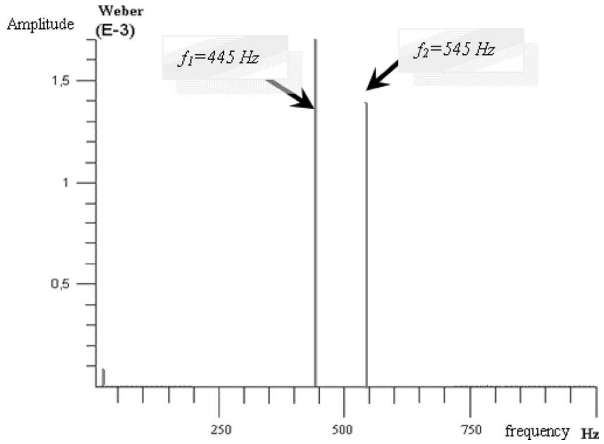

Fig. 7. Spectrum of the hf ripple in the magnetizing flux at no load.

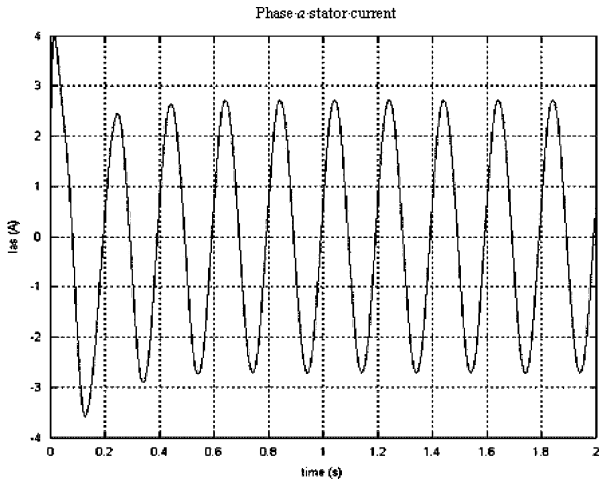

Fig. 8. Phase a stator current without injection at no load.

frequencies:

$$f_1 = f_{\rm rot} - f_{\rm osc} - f_e = 445\,{\rm Hz}$$
$$f_2 = f_{\rm rot} + f_{\rm osc} - f_e = 545\,{\rm Hz} \qquad (25)$$

as shown in Fig. 7. In particular, if $f_{\rm osc} = 0$ and $f_{\rm rot} = f_{\rm hf}$, the amplitude of the air-gap flux contains only the harmonic

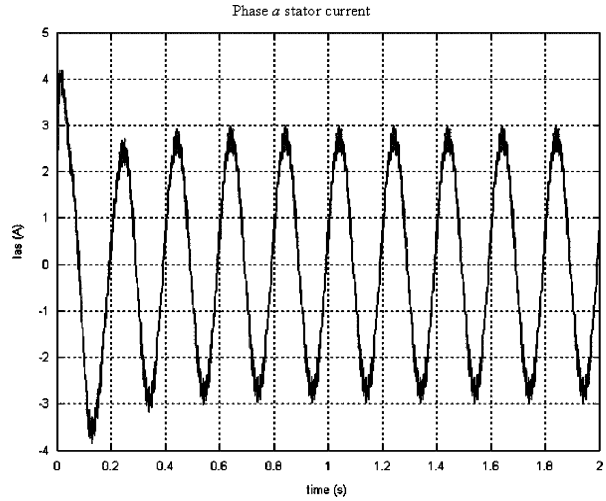

Fig. 9. Phase a stator current with injection at no load.

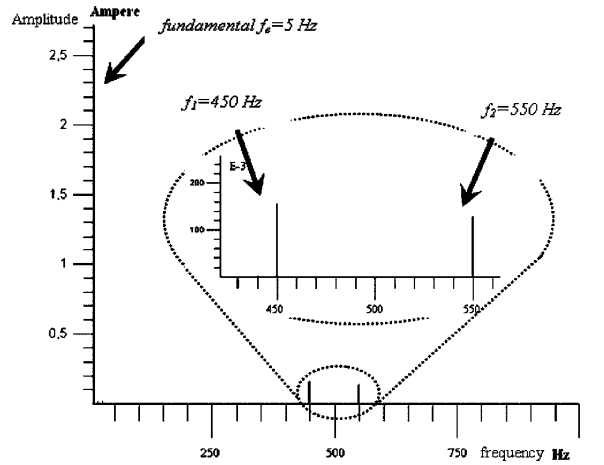

Fig. 10. Spectrum of the stator phase a current with injection at no load.

at frequency $f_{\rm hf} - f_e$ [13], which can be used in sensorless control to determine the position of the magnetizing flux [14]. It should be noted that the curves in Figs. 5 and 6 show only the fundamental component of the magnetizing flux, from which the third harmonic component is created using the curve in Fig. 2.

The flux linking both the stator slots and the rotor bars induces hf currents into them. Indeed, analyzing the phase a stator current, shown in Figs. 8 and 9, the effects of the ripple due to the injected signal are clearly illustrated by additional hf harmonics (Fig. 9).

In particular, the spectrum of the phase a stator current is characterized by two additional harmonics, shown in Fig. 10, respectively, at frequencies

$$f_1 = f_{\rm rot} - f_{\rm osc} = 450\,Hz$$
$$f_2 = f_{\rm rot} + f_{\rm osc} = 550\,Hz \qquad (26)$$

The electromagnetic torque produced by the motor, which contains the effects of the normal rotor circuit and the third harmonic rotor circuit as well as the motor speed is shown in Figs. 11 and 12.

In particular, in Fig. 11, the effect of saturation is seen easily, which causes a ripple in the motor torque and speed oscillations

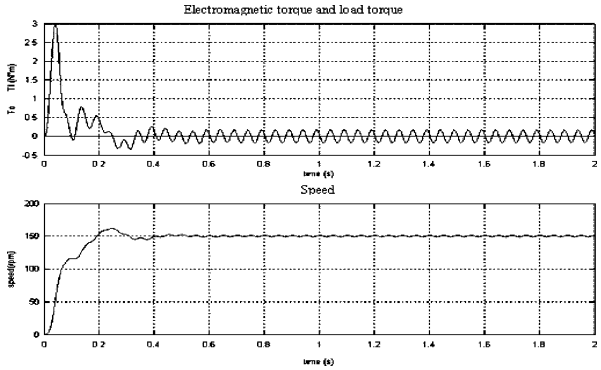

Fig. 11. Electromagnetic torque and rotor speed without hf injection at no load.

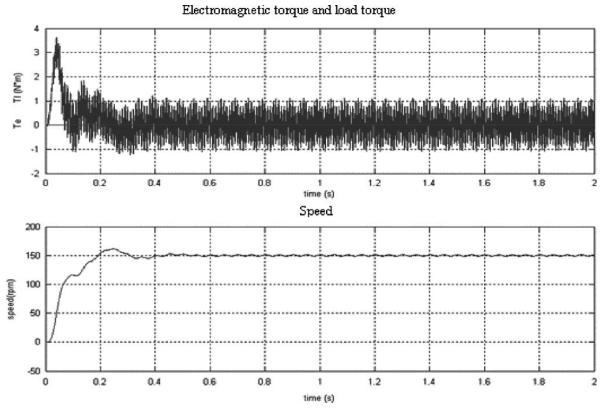

Fig. 12. Electromagnetic torque and rotor speed with hf injection at no load.

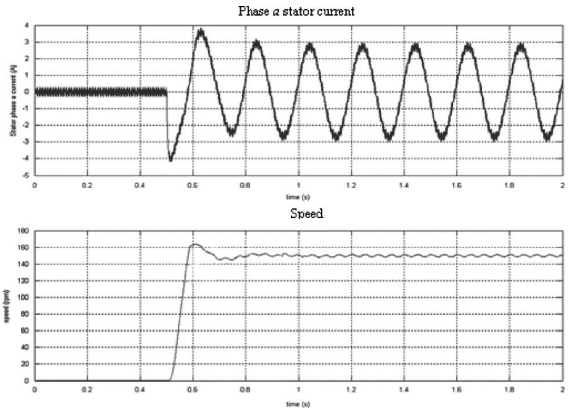

Fig. 13. Phase a stator current and rotor speed at no load.

due to the third harmonic air-gap flux component. Fig. 12 shows the effects of the additional hf signal that creates an hf ripple in the torque value but that has almost no effect on the motor speed because of the rotor inertia.

Fig. 13 shows how the phase a stator current and the rotor speed vary at no load when the reference speed changes from zero to $\omega_r = 15.71$ rad/s. It is readily seen that the added signal has no effect on the rotor speed transient behavior.

B. Full Load Tests

To evaluate the effects of the hf injection with an impressed load torque, simulation runs were performed using a 32.5 $V_{\rm rms}$,

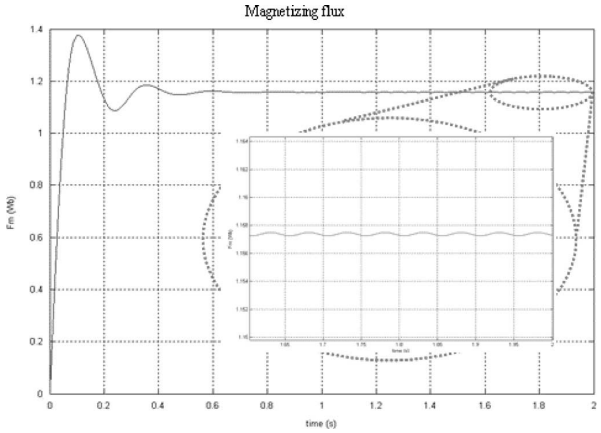

Fig. 14. Magnetizing flux λ_m without injection at full load.

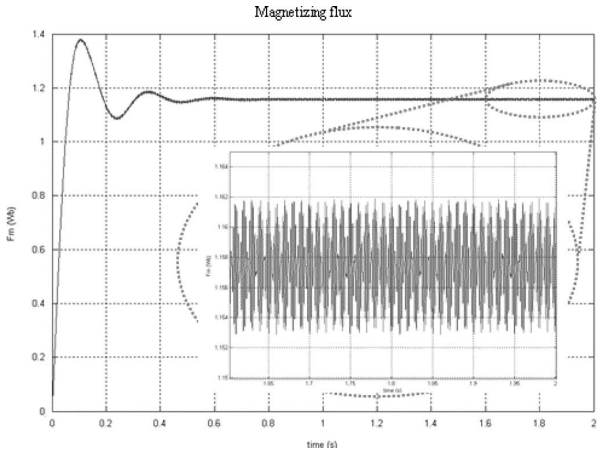

Fig. 15. Magnetizing flux λ_m with injection at full load.

5 Hz balanced set as supply voltages and the 20 $V_{\rm rms}$, 500 Hz balanced set modulated in amplitude at 50 Hz as the additional signal. A constant torque $T_l = 7.5$ Nm was adopted as the motor load. Figs. 14 and 15 show the amplitude of the air-gap flux without and with the additional hf signal: the ripple due to the injected signal can be observed easily (Fig. 15); such a ripple, characterized again by the two additional harmonics in (25), shown in Fig. 16, does not modify the mean value of the amplitude of the magnetizing flux ($\lambda_m = 1.157$ Wb, which is equal to the no load simulation value. Similarly to no-load operation, the flux linking the stator slots induces an hf ripple in the stator currents, whose spectrum is again characterized by two additional harmonics, shown in Fig. 17, respectively, at the frequencies reported in (26).

Finally, the electromagnetic torque and rotor speed are shown in Figs. 18 and 19, showing the same effects as at no load.

In particular, in Fig. 18, one can easily see the effect of saturation that causes a ripple in the motor torque and oscillations in the speed due to the third harmonic air-gap flux component. Fig. 19 shows the effects of the additional hf signal that creates an hf ripple in the torque value but that has almost no effect on the motor speed because of the rotor inertia.

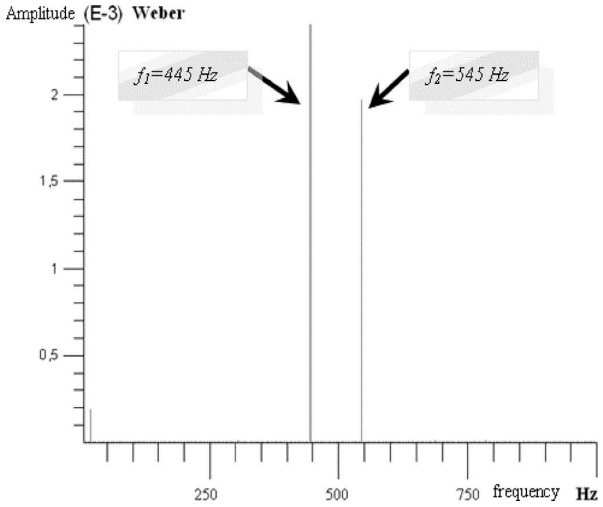

Fig. 16. Spectrum of the hf ripple in the magnetizing flux at full load.

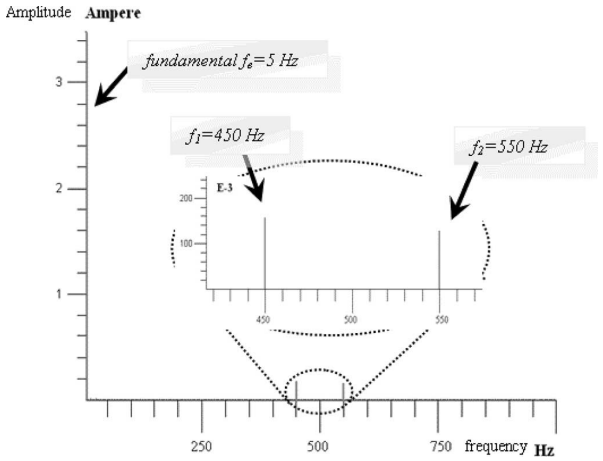

Fig. 17. Spectrum of the stator phase a current with injection at full load.

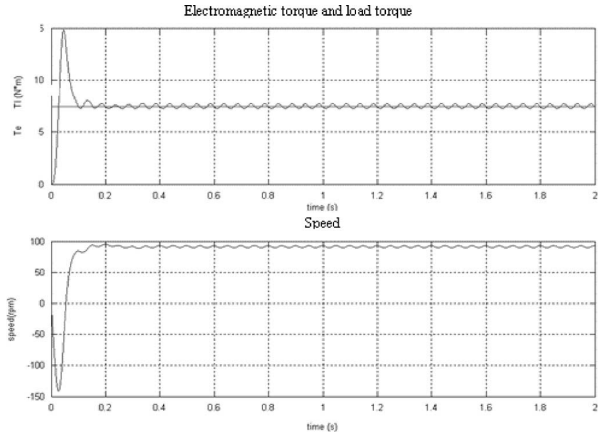

Fig. 18. Electromagnetic torque and rotor speed without hf injection at full load.

V. Experimental Results

Experimental measurements were also performed to verify the simulation model. Using the same IM modeled in Section IV, the signal in (20) is added to the normal inverter source.

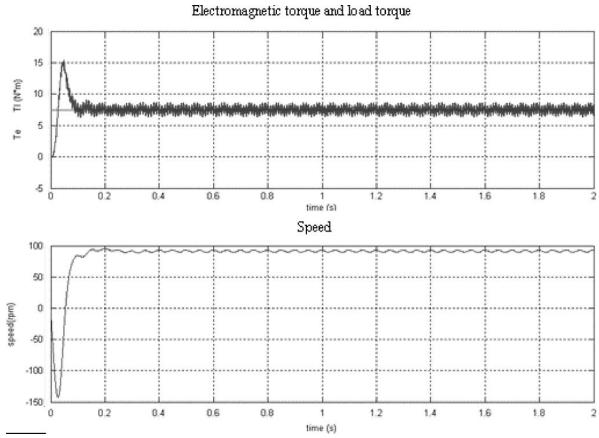

Fig. 19. Electromagnetic torque and rotor speed with hf injection at full load.

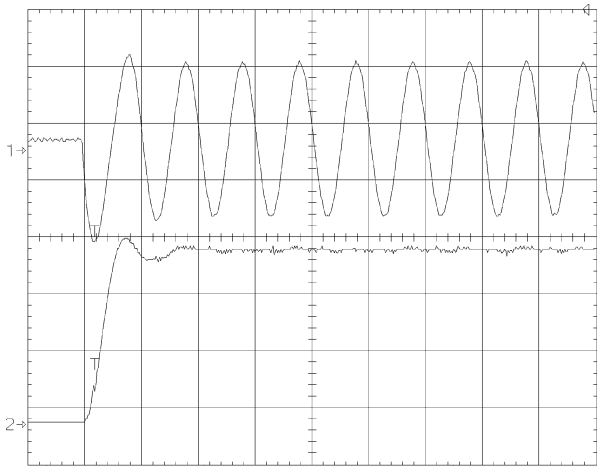

Fig. 20. Phase a stator current and rotor speed at no load (experimental result): time (200 ms/div), current (2A/div), speed [50 (r/min)/div].

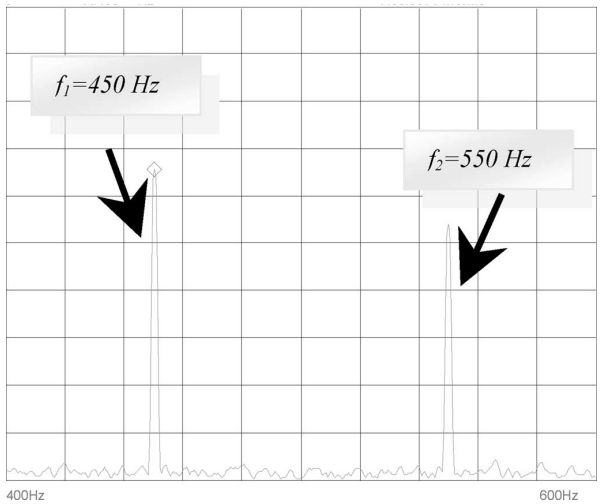

Fig. 21. Spectrum of phase a stator current hf ripple at no load: frequency (20 Hz/div), amplitude (25 mA/div).

Fig. 20 shows how the phase a stator current and the rotor speed vary at no load when the reference speed changes from zero to $\omega_r = 15.71$ rad/s, while Fig. 21 shows the phase a stator current spectrum at steady state. Analyzing Figs. 13 and 20, one

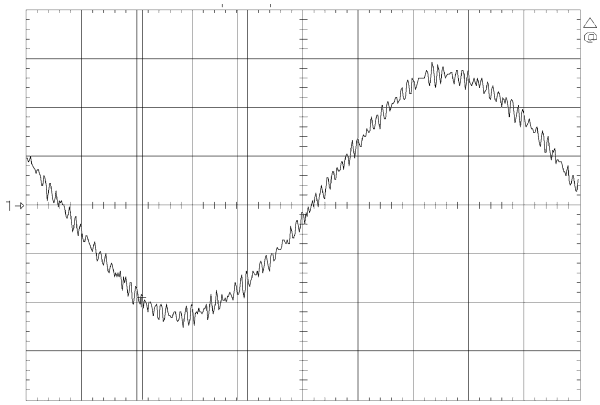

Fig. 22. Phase a stator current at full load: time (20 ms/div), current (1.5A/div).

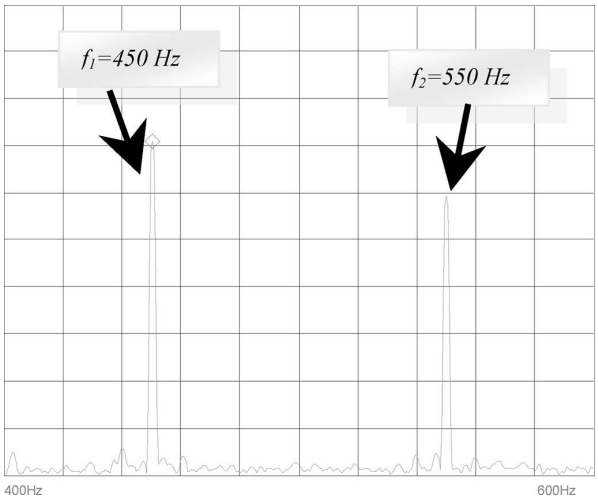

Fig. 23. Spectrum of phase a stator current hf ripple at full load: frequency (20 Hz/div), amplitude (25 mA/div).

can observe the same dynamic response of the analytical model and the experimental system. Obviously, the hf added signal does not modify the dynamic response of the system.

It can be easily seen that the rotor speed is not affected by any hf ripple due to the signal injected but only by a third harmonic ripple due to saturation. On the contrary, the phase a stator current contains the two additional harmonics shown in Fig. 21 and predicted in (26).

Figs. 22 and 23 show the phase a stator current and its hf ripple spectrum at full load.

VI. Conclusion

A new model for an induction motor, able to take into account the effects due to the interaction of saturation and additional hf fields, has been described in this paper. This improved d–q model is derived from the two models described in [6] and [10], and is based on the fact that saturation introduces both a third harmonic component and a decreasing amplitude of the fundamental component of the magnetizing flux. Therefore, it is necessary to introduce both a saturation factor and a third harmonic of the air-gap flux that is derived from the fundamental component that induces third harmonic currents in the rotor circuit. The resulting model is able to describe one of the main effects of signal injection that can be summarized in the modulation of the saturation level.

Simulation tests using an additional magnetic field pulsating at $\omega_{\rm osc}$ and rotating at $\omega_{\rm rot}$ have been performed. Apart from the creation of harmonics that contain information about the position of the flux, modulation of the machine saturation level introduces a ripple in the stator currents and in the motor torque depending on the angular frequency of the injected signal, but shows no effects on the rotor speed.

References

[1] A. Consoli, G. Scarcella, and A. Testa, "A new zero-frequency flux position detection approach for direct-field-oriented-control drives," *IEEE Trans. Ind. Appl.*, vol. 36, no. 3, pp. 797–804, May/Jun. 2000.

[2] F. Briz, M. W. Degner, P. Garcia, and R. D. Lorenz, "Comparison of saliency-based sensorless control techniques for AC machines," *IEEE Trans. Ind. Appl.*, vol. 40, no. 4, pp. 1107–1115, Jul./Aug. 2004.

[3] J. I. Ha and S. K. Sul, "Sensorless field orientation control of an induction machine by high frequency signal injection," *IEEE Trans. Ind. Appl.*, vol. 35, no. 1, pp. 45–51, Jan./Feb. 1999.

[4] J. A. A. Melkebeek and D. W. Novotny, "The influence of saturation on induction machine drive dynamics," *IEEE Trans. Ind. Appl.*, vol. IA-19, no. 5, pp. 671–681, Sep./Oct. 1983.

[5] Y. He and T. A. Lipo, "Computer simulation of an induction machine with spatially dependent saturation," *IEEE Trans. Power App. Syst.*, vol. PAS-103, no. 4, pp. 707–714, Apr. 1984.

[6] T. A. Lipo and A. Consoli, "Modelling and simulation of induction motors with saturable leakage reactances," *IEEE Trans. Ind. Appl.*, vol. IA-20, no. 1, pp. 180–189, Jan./Feb. 1984.

[7] J. O. Ojo, T. A. Lipo, and A. Consoli, "An improved model of saturated induction machines," *IEEE Trans. Ind. Appl.*, vol. 26, no. 2, pp. 212–221, Mar./Apr. 1990.

[8] C. H. Lee, "Saturation harmonics of polyphase induction machines," *Trans. AIEE*, vol. 80, pp. 597–603, Oct. 1961.

[9] B. J. Chalmers and R. Dodgson, "Waveshapes of flux density in polyphase induction motors under saturated conditions," *IEEE Trans. Power App. Syst.*, vol. PAS-90, no. 2, pp. 564–569, Mar. 1971.

[10] J. C. Moreira and T. A. Lipo, "Modeling of saturated ac machines including air gap flux harmonic components," *IEEE Trans. Ind. Appl.*, vol. 28, no. 2, pp. 343–349, Mar./Apr. 1992.

[11] T. A. Lipo and Y. Liao, "Effect of saturation third harmonic on the performance of squirrel-cage induction machines," *Electr. Mach. Power Syst.*, vol. 22, no. 2, pp. 155–73, Mar./Apr. 1994.

[12] A. Consoli, G. Scarcella, G. Scelba, A. Testa, and D. Triolo, "Low frequency signal demodulation-based sensorless technique for induction motor drives at low speed," *Trans. Ind. Electron.*, vol. 53, no. 1, pp. 1–9, Feb. 2006.

[13] A. Consoli, G. Scarcella, G. Bottiglieri, and A. Testa, "Saturation modulation in voltage zero sequence-based encoderless techniques. Part I: Harmonic analysis," in *Proc. IEEE Int. Conf. Electron. Mach. Drives (IEMDC)*, San Antonio, TX, May 15–18, 2005, pp. 950–956, (in CD ROM).

[14] A. Consoli, G. Scarcella, G. Scelba, S. Royak, and M. M. Harbaugh, "Saturation modulation in voltage zero sequence-based encoderless techniques. Part II: Implementation issues," in *Proc. IEEE IEMDC*, San Antonio, TX, May 15–18, 2005, pp. 2017–2023, (in CD ROM).

Giovanni Bottiglieri (S'98) was born in Scicli, Italy, in 1978. He received the M.S. degree in electrical engineering in 2002 from the University of Catania, Catania, Italy, where he is currently working toward the Ph.D. degree.

His current research interests include electric machines and sensorless controls of electrical drives.

Alfio Consoli (M'79–SM'88–F'00) was born in Catania, Italy. He received the Graduate degree in electrical engineering from the Politecnico di Torino, Turin, Italy.

During 1973–1974, he was with FIAT, Torino, Italy. In 1975, he joined the Department of Electrical, Electronic, and Systems Engineering, University of Catania, Catania, where he has been a Professor of electrical engineering since 1985 and the Coordinator of the scientific activities of Ph.D. candidates in electrical engineering since 1987. He is engaged in the areas of electrical machines and power electronics. His current research interests include energy conversion systems, electrical drives, robotics, and power electronics. During 1985, he was a Visiting Professor of electromagnetic design at the University of Wisconsin, Madison. He holds three international patents, two of them on sensorless control of drives. He is the coauthor and coeditor of the book *Modern Electric Drives* (Amsterdam, The Netherlands: Kluwer, 2000). He is also the author of *Electrical Motors* (the Italian National Encyclopedy "Treccani," Appendix V, vol. III, pp. 564–575).

Prof. Consoli received a NATO Grant at Purdue University, West Lafayette, IN, in 1980. He is also the recipient of the Third Prize for the paper presented at the *IEEE-IAS Annual Meeting* in 1998 and the Best Paper Award for publication in the *IEEE Transactions on Power Electronics* in 2000, both for papers on sensorless control of ac motor drives. He was one of the Distinguished Lecturers for the period 2002–2004. From 1997 to 2001, he was a member of the Executive Board of the IEEE Industry Application Society. He is a member of the Executive Committee of the IEEE Power Electronics Society, where he is currently the Chairman of the Technical Committee on Motor Drives. He is also an Associate Editor of the *IEEE Transactions on Power Electronics*. He is the President of the Converters, Machines, and Electrical Drives (CMAE)—the Association of the Italian Professors on Power Electronics. He is also a member of the Italian Electric Association and European Power Electronics Association.

Thomas A. Lipo (M'64–SM'71–F'87–LF'04) was born in Milwaukee, WI. He received the B.E.E. and M.S.E.E. degrees from Marquette University, Milwaukee, WI, in 1962 and 1964, respectively, and the Ph.D. degree in electrical engineering from the University of Wisconsin (UW), Madison, in 1968.

From 1969 to 1979, he was an Electrical Engineer in the Power Electronics Laboratory, Cooperate Research and Development, General Electric Company, Schenectady, NY. In 1979, he joined Purdue University, West Lafayette, IN, as a Professor of electrical engineering. In 1981, he joined UW as a Professor, where he is currently the W. W. Grainger Professor of Power Electronics and Electrical Machines.

Dr. Lipo has received the Outstanding Achievement Award from the IEEE Industry Applications Society, in 1986, the William E. Newell Award of the IEEE Power Electronics Society, in 1990, and the 1995 Nicola Tesla IEEE Field Award from the IEEE Power Engineering Society. He has been the President of the IEEE Industry Applications Society. He is a Fellow of the Institution of Electrical Engineers, U.K., a member of the Institute of Electrical Engineers of Japan, and a Fellow of the Royal Academy of Great Britain.